Carbohydrate Polymers 90 (2012) 1216–1225

Contents lists available at SciVerse ScienceDirect

Carbohydrate Polymers

journal homepage: www.elsevier.com/locate/carbpol

Natural polymer-based magnetic hydrogels: Potential vectors for remote-controlled drug release

Alexandre T. Paulino[a,b,c,*], Antonio G.B. Pereira[d], André R. Fajardo[d], Kristin Erickson[b], Matt J. Kipper[b], Edvani C. Muniz[d], Laurence A. Belfiore[b], Elias B. Tambourgi[a]

[a] School of Chemical Engineering, Department of Chemical System Engineering, Separation Process Laboratory, State University of Campinas, Av. Albert Einstein, 500, Bloco A, Cidade Universitária, Campinas, SP 13083-852, Brazil
[b] Department of Chemical & Biological Engineering, Polymer Physics & Engineering Laboratory, Colorado State University, Fort Collins, CO 80523, USA
[c] Department of Food Engineering, Higher Education Center of the West, Santa Catarina State University, Chapecó/Pinhalzinho, SC 89870-000, Brazil
[d] Department of Chemistry, Polymer Material & Composite Laboratory (GMPC-UEM), Av. Colombo, 5790, Maringá, PR 87050-900, Brazil

ARTICLE INFO

Article history:
Received 30 April 2012
Received in revised form 15 June 2012
Accepted 18 June 2012
Available online 26 June 2012

Keywords:
Polysaccharide
Magnetic hydrogel
Swelling
Controlled release
Curcumin
Magnetite

ABSTRACT

The preparation and characterization of natural polymer-based hydrogels that contain 50-nm diameter magnetite (i.e., $FeO:Fe_2O_3$) nanoparticles are described herein. Fourier-transform infrared spectroscopy (FTIR) analysis confirmed the efficiency of the polysaccharide-modifying process. Thermogravimetric analysis (TGA), differential scanning calorimetry (DSC), and compressive moduli demostrate that the presence of magnetite improves thermal and mechanical resistance. Transient diffusion of water in magnetic hydrogels was analyzed via boundary layer mass transfer across an expaning interface, and the degree of swelling of these polysaccharide hydrogels decreases in the presence of magnetite, with no variation in the binary diffusion mechanism. The absence of hysteresis loops and coercivity observed via magnetometry suggests that magnetic hydrogels are useful for remote-controlled drug release, as demonstrated by magnetic-field-induced release of curcumin. Experiments reveal that magnetic hydrogels with greater magnetic susceptibility have the potential to release larger concentrations of drugs from the hydrogel network.

1. Introduction

Recently, there has been substantial interest in the potential applications of functionalized hydrogels. These materials have many important properties and offer advantages over non-functionalized hydrogels (Bajpai, Shukla, Bhanu, & Kankane, 2008; Chaterji, Kwon, & Park, 2007). The advantages of functionalized hydrogels have been determined in studies of controlled drug release, cell proliferation, water treatment, soil conditioning, etc. (Arizaga, Ibarz, & Piñol, 2010; Deligkaris, Tadele, Olthuis, & van den Berg, 2010; Oh, Drumright, Siegwart, & Matyjaszewski, 2008).

Hydrogels can be functionalized by using a variety of additives, such as non-arginine cell-penetrating peptides (Liu et al., 2009), organic or inorganic complex counterions (Friedrich, Trinker, & Tieke, 2010), and aniline oligomers (Baolin, Anna, & Ann-Christine, 2011), and magnetite (Paulino, Belfiore, Kubota, Muniz, Almeida et al., 2011; Paulino et al., 2009; Paulino, Guilherme, Mattoso, & Tambourgi, 2010). The addition of magnetite to polymer hydrogel networks yields a new class of functionalized materials widely known as magnetic hydrogels, whose most important characteristic is magnetic sensitivity (Lau et al., 2009; Snyder, Nguyen, & Ramanujan, 2010a,b). Magnetic hydrogels have been investigated and applied in remote-controlled drug release, cancer treatment, ion recovery, etc. (Lau et al., 2009; Paulino, Belfiore, Kubota, Muniz, & Tambourgi, 2011; Snyder et al., 2010a,b). Some specific functionalized hydrogels are known as smart hydrogels, because they can be activated via external stimuli (e.g., pH variation, ionic strength, temperature, magnetic field, etc.) (Chatterjee, Haik, & Jen, 2003; Deng, Yang, Wang, & Fu, 2003). These smart hydrogels are known as pH-sensitive, ionic-strength-sensitive, temperature-sensitive, and magnetic-field-sensitive hydrogels, respectively (Paulino et al., 2010; Snyder et al., 2010a).

Natural polymer-based functionalized hydrogels, such as polysaccharides, proteins, and amino acids, have been studied extensively for medical, pharmaceutical, and biological applications due to their biocompatibility with living organisms, biodegradability, accessibility, and renewability (Mahkam, 2010; Song, Zhang, Shi, & Li, 2010; Wang et al., 2010). In some cases, it is necessary to improve the thermal and mechanical stability

* Corresponding author at: School of Chemical Engineering, Department of Chemical System Engineering, Separation Process Laboratory, State University of Campinas, Av. Albert Einstein, 500, Bloco A, Cidade Universitária, Campinas, SP 13083-852, Brazil. Tel.: +55 19 3521 3952; fax: +55 19 3521 3894.
E-mail address: atpaulino10@gmail.com (A.T. Paulino).

0144-8617/$ – see front matter © 2012 Elsevier Ltd. All rights reserved.
http://dx.doi.org/10.1016/j.carbpol.2012.06.051

of these hydrogels (Gutowska, Bae, Jacobs, Feijen, & Kim, 1994; Paulino, Fajardo, Junior, Muniz, & Tambourgi, 2011; Shalviri, Liu, Abdekhodaie, & Wu, 2010; Simionato, Paulino, Garcia, & Nozaki, 2006). Problems associated with poor thermal and mechanical stability might be addressed via the incorporation of magnetite during hydrogel synthesis, which corrects these deficiencies and introduces magnetic sensitivity. All of these properties are extremely important for applications of natural polymer-based functionalized hydrogels in remote-controlled drug release, as well as other biological, chemical, and pharmaceutical applications (Gutowska et al., 1994; Shalviri et al., 2010).

This research contribution describes the preparation of natural polymer-based magnetic hydrogels that contain $FeO{:}Fe_2O_3$ nanoparticles in the polymer network. The addition of magnetite to these hydrogels improves thermal and mechanical properties, in the presence of magnetic sensitivity. Gum arabic (GU), chitosan (CS), and maltodextrin (MA) were used as natural polymers. Magnetic hydrogels were characterized by Fourier-transform infrared spectroscopy (FTIR), thermogravimetric analysis (TGA), differential scanning calorimetry (DSC), magnetometry, and stress–strain testing under compression. The water diffusion mechanism was analyzed and remote-controlled release of curcumin was investigated to confirm the applicability of these materials as new vectors in remote-controlled drug release.

2. Materials and methods

2.1. Reagents

Chitosan (CS, Aldrich), acetic acid (Ac, Merck), acrylic acid (AAc, Merck), glycidyl methacrylate (GMA, Across Organics), methylenebisacrylamide (MBA), hydrochloric acid (HCl, Merck), ammonium persulfate (APS, Aldrich), gum arabic (GU, Company, Sudan), sodium hydroxide (NaOH, Nuclear), acrylamide (AAm, Aldrich), potassium acrylate (KAAc, Aldrich), maltodextrin (MA, Aldrich), ethanol (TEDIA), tetrahydrofuran (THF, Sigma–Aldrich), curcumin (CUR, Sigma–Aldrich), and magnetite nanoparticles ($FeO{:}Fe_2O_3$, 50-nm diameter) were purchased from Fisher Scientific and have been characterized elsewhere (Paulino et al., 2009). All experiments were performed using Milli-Q® water.

2.2. Preparation of natural polymer-based magnetic hydrogels

CS-based hydrogels were synthesized by employing the following procedure: 1% CS solution was prepared by diluting 0.3 g polysaccharide with 30.00-mL 1% acetic acid in a 50-mL beaker. Next, the solution was transferred to a 250-mL four-neck flask equipped with a mechanical stirrer, reflux condenser, funnel, and nitrogen line. Nitrogen was purged into the system for 30 min to remove dissolved oxygen. Then, 0.5215 mmol APS was introduced to generate free radicals in CS. After 10 min, a solution containing 15 mL of water, 3.40 mL of AAc, MBA, and magnetite nanoparticles was added to CS, and the cross-linking reaction was performed at 70 °C for 3 h. The crosslinked CS hydrogel was transferred to a 250-mL beaker containing 2 mol L^{-1} of sodium hydroxide solution and neutralized for 15 min. The CS hydrogel was dried at 50 °C for 12–24 h.

Prior to synthesizing hydrogels based on either GU or MA, the specific polysaccharide was functionalized using glycidyl methacrylate, GMA (van Dijk-Wolthuis et al., 1995; van Dijk-Wolthuis, Kettenes-van den Bosch, van der Kerk-van Hoof, & Hennink, 1997). This procedure was carried out with slight modification relative to the recipe described in the above-mentioned publication. Either 12 g of purified malto-dextrin (P-MA) or purified gum arabic (P-GU) was dissolved in a 500-mL beaker containing 480 mL of distilled water at 60 °C and pH = 3.50. After adding GMA and stirring for 24 h, the resultant polysaccharide was precipitated in ethanol three times, obtaining either modified malto-dextrin (M-MA) or modified gum arabic (M-GU). The natural polymer-based hydrogels were synthesized utilizing these modified polysaccharides. Each synthesis was performed via solubilization of the modified polysaccharide in aqueous solution containing AAm, KAAc, APS, and magnetite nanoparticles. These solutions were heated to 65 °C for 90 min under constant stirring. Crosslinked hydrogels were immersed in Milli-Q® water for washing, with fresh water introduced every 8 h during 9 cycles, for a total period of 72 h. The mass fraction of magnetite in the hydrogels was established and controlled in relation to the total mass of the reagents.

2.3. Degree of swelling

Dried hydrogels of known mass were placed in contact with a specified volume of water for various contact times, with pH controlled at approximately 6.5. For each contact time, the wet mass of each swollen hydrogel was measured to calculate the degree of swelling (DS) according to Eq. (1):

$$\mathrm{DS} = \frac{m_{\mathrm{swollen}} - m_{\mathrm{dry}}}{m_{\mathrm{dry}}} \tag{1}$$

in which m_{swollen} and m_{dry} are the masses of swollen and dried hydrogels, respectively.

Eq. (1) for DS is analogous to engineering strain in mechanical testing. A better definition of DS that parallels the integral expression for true strain is given by Eq. (2):

$$\mathrm{DS}_{\mathrm{true}} = \int_{m_{\mathrm{dry}}}^{m_{\mathrm{swollen}}} \frac{dm}{m} = \ln\left\{\frac{m_{\mathrm{swollen}}}{m_{\mathrm{dry}}}\right\} = \ln\left\{\frac{m_{\mathrm{dry}} + \Delta m}{m_{\mathrm{dry}}}\right\}$$
$$= \ln\left\{1 + \frac{\Delta m}{m_{\mathrm{dry}}}\right\} = \frac{\Delta m}{m_{\mathrm{dry}}} - \frac{1}{2!}\left\{\frac{\Delta m}{m_{\mathrm{dry}}}\right\}^2 + \cdots \tag{2}$$

Eq. (1) for the "engineering degree of swelling" is valid if $\Delta m/m_{\mathrm{dry}}$ is small enough that the quadratic term is negligible in comparison to the linear term in Eq. (2). For DS greater than 100% (i.e., DS > 1), $\mathrm{DS}_{\mathrm{true}}$ in Eq. (2) is probably a better representation of the degree of swelling than DS in Eq. (1).

The diffusion exponent (n) is a scaling parameter that describes the water diffusion mechanism in hydrogels (Zhang, Wu, Li, & Wang, 2005). Logarithmic graphs of the fractional mass of water absorbed in hydrogels, $m(t)/m_{\mathrm{equilibrium}}(t \Rightarrow \infty)$, vs. time t yield exponent n in Eq. (3). Scaling exponents n were calculated via log–log analysis of Eq. (3) (Brazel & Peppas, 1999):

$$\frac{m(t)}{m_{\mathrm{equilibium}}(t \Rightarrow \infty)} = kt^n \tag{3}$$

in which $m(t)$ and $m_{\mathrm{equilibrium}}(t \Rightarrow \infty)$ are the absorbed masses of water in hydrogels at time t and at equilibrium, respectively, and rate constant k, with dimensions of $(\mathrm{time})^{-n}$, is proportional to the square-root of the molecular diffusion coefficient of water in polymeric hydrogels, according to the classic penetration theory of boundary layer mass transfer.

2.4. Infrared spectroscopy (FTIR)

FTIR spectra of natural polymer-based hydrogels were obtained in compressed potassium bromide pellets (FT-GO_{max} Bomem Easy MB-100, Nickelson). To achieve the best resolution (4.0 cm^{-1}), 16 scans per minute were recorded, and 64 interferograms were signal-averaged prior to Fourier transformation.

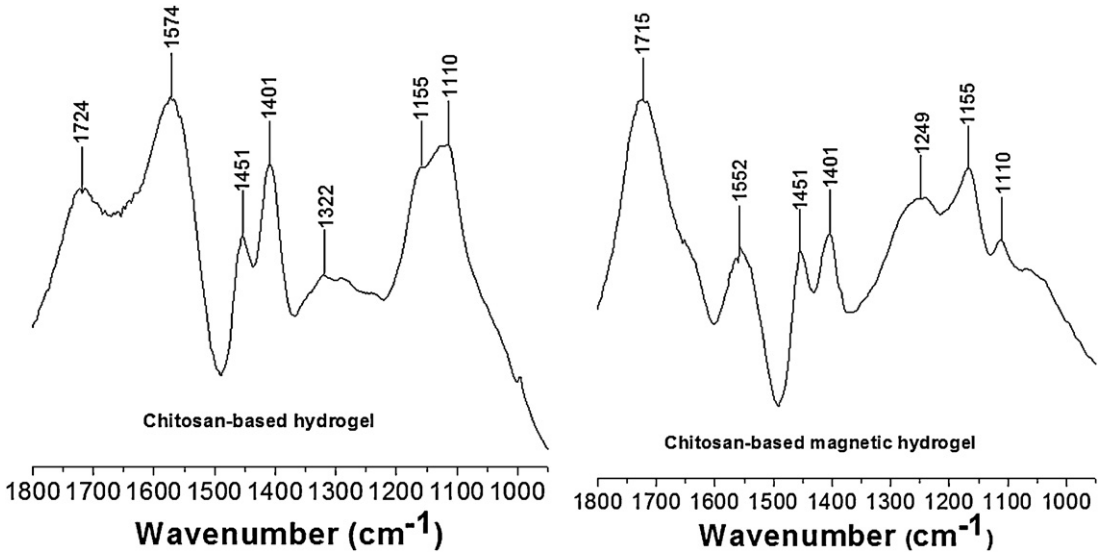

Fig. 1. Transmission FTIR spectra of CS-based hydrogels, with and without FeO:Fe_2O_3 nanoparticles.

2.5. Magnetometry

Magnetization curves for polysaccharide-based magnetic hydrogels were measured using a vibrating-sample magnetometer (physical properties measurement system PPMS-9, Quantum Design with a SQID magnetometer), with a maximum magnetic field of 7 T and sensitivity of 10^{-6} emu at 573 K. To determine coercivity, samples were cooled initially under zero-field conditions from ambient temperature to the measuring temperature. Dry natural polymer-based magnetic hydrogels were positioned on quartz holders and placed in the magnetometer. Magnetization vs. magnetic field was generated by varying the magnetic field.

2.6. Thermal analysis (DSC and TGA)

DSC analyses were carried out on a Shimadzu calorimeter (Model DSC 50, Japan). TGA analyses were performed on a Shimadzu calorimeter (Model TGA 50, Japan). Both calorimetric experiments were performed at a heating rate of 10 °C min^{-1} under a nitrogen flow rate of 10 mL min^{-1} over the following temperature ranges: 25–400 °C for DSC, and 25–1000 °C for TGA.

2.7. Stress vs. strain under compressive loads

Natural polymer-based magnetic hydrogels were cut into small cylinders, dried, weighed, and immersed in a cylindrical container containing 50 mL distilled H_2O at room temperature for 48 h. After equilibrium swelling was achieved, samples were removed from the aqueous environment and the modulus of elasticity (E) was calculated via compression tests (Texturometer–Stable TA.XT2 texture analyzer equipped with a 5-kg load cell). Other parameters of the texturometer: 5-mm indentation profundity, 1-mm s^{-1} downward probe velocity, and initial cross-sectional area of 126 mm^2. The compression tests were performed quickly at ambient temperature to prevent loss of the liquid absorbed in the hydrogel network. The texturometer measures force (F) vs. deformation. These data were analyzed via Eq. (4) to calculate the compressive modulus of elasticity E (Gutowska et al., 1994):

$$\sigma_{\text{engineering}} = \frac{F}{A_{\text{initial}}} = E\left\{\lambda - \frac{1}{\lambda^2}\right\} \quad (4)$$

in which $\sigma_{\text{engineering}}$ is the engineering compressive stress relative to the sample's initial cross-sectional area A_{initial}, and λ is the compression ratio relative to the initial thickness L_{initial}, according to Eq. (5):

$$\lambda = \frac{L}{L_{\text{initial}}} \quad (5)$$

where L is the compressed sample thickness. Compressive modulus of elasticity E is (i) one-third of the initial slope of $\sigma_{\text{engineering}}$ vs. λ (i.e., $\{d\sigma_{\text{engineering}}/d\lambda\}_{\lambda=1}$), or (ii) the linear-least-squares slope of $\sigma_{\text{engineering}}$ vs. $\{\lambda - 1/\lambda^2\}$.

2.8. Remote-controlled release of curcumin

2.8.1. Microsphere loading

During the loading step of CUR, 1.25 mg of this drug was dissolved in a 250-mL flask containing 100 mL aqueous solution of THF (i.e., 1:1 ratio with distilled H_2O). 1 g of hydrogel was added to this solution in the presence of constant stirring for 48 h at ambient temperature until the hydrogel achieved equilibrium swelling. Then, the supernatant was removed and analyzed using UV–visible spectrophotometry (Fenton, model 800Xi apparatus) at 430 nm to estimate the loading efficiency, according to Eq. (6). The concentration of CUR that diffused into the hydrogel was calculated based on the initial amount of CUR in solution without hydrogel, and the residual amount of CUR in solution after the establishment of hydrogel swelling equilibrium. CUR concentrations were calculated using a calibration curve determined previously from standard CUR solutions. The CUR concentration range in distilled H_2O/THF (ratio 1:1) without hydrogel, used to generate the calibration curve, was between 1.28×10^{-3} g/L and 7.68×10^{-3} g/L, with a linear correlation coefficient (R^2) of 0.9995. The encapsulation efficiency was calculated using Eq. (6):

$$\text{Encapsulation efficiency} = \frac{\text{CUR}(t=0) - \text{CUR}(t \Rightarrow \infty)}{\text{CUR}(t=0)} \quad (6)$$

in which CUR(t = 0) is the initial concentration of CUR in solution without hydrogel, and CUR($t \Rightarrow \infty$) is the residual concentration of CUR in the supernatant after the hydrogel achieves equilibrium swelling.

2.8.2. In vitro controlled release of curcumin

In vitro controlled CUR release studies were performed using a phosphate buffer solution (pH 7.4) and dissolution apparatus. Known masses of hydrogels containing encapsulated CUR were

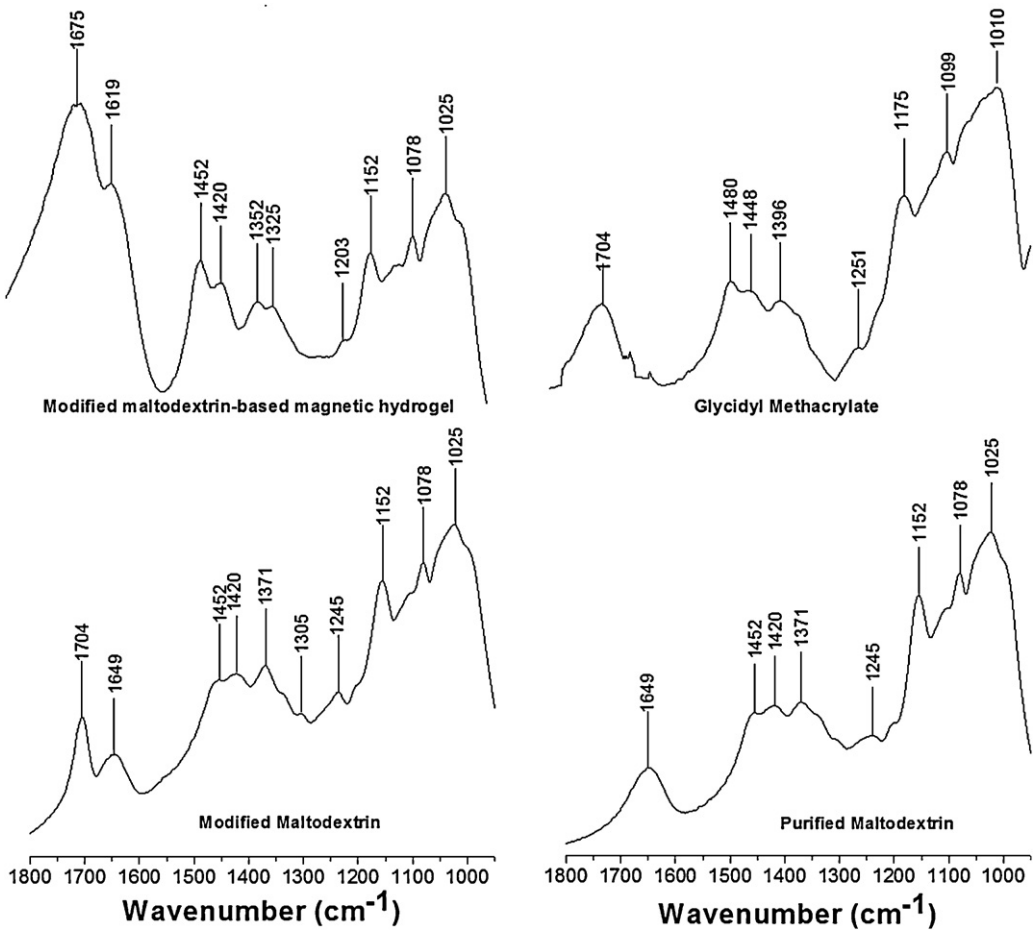

Fig. 2. Transmission FTIR spectra of P-MA modified with GMA, and M-MA-based hydrogels, with and without FeO:Fe_2O_3 nanoparticles.

added to flasks containing specified volumes of the phosphate buffer solution at ambient temperature. At specific time intervals, 3-mL aliquots of buffer solution were analyzed to determine the fraction of CUR released. CUR concentration was calculated via UV–visible spectrophotometry and the calibration curve, as described in the previous section. The released CUR fraction was calculated according to Eq. (7):

$$\text{Fraction released} = \frac{\text{amount released}}{\text{amount encapsulated}} \tag{7}$$

3. Results and discussion

3.1. Hydrogel swelling kinetics

The degree of swelling (DS) decreased from 8.8 to 6.5 g of water per gram of CS-based dried hydrogel concurrently with the increase in magnetite concentration from 0.0 to 5.5 wt.%, respectively. As a consequence of iron chelation to polysaccharide functional groups, the degree of swelling of CS-based magnetic hydrogels was less than that for CS-based hydrogels without magnetite. Taking into account the magnitude of DS, it seems reasonable that the "true degree of swelling" described by Eq. (2) is more accurate for this kind of hydrogel. The same behaviour was observed with M-MA-based and M-GU-based hydrogels, as a lesser degree of swelling occurred in the presence of magnetite, and the "true degree of swelling" provided a better representation of the absorption of water in all of the hydrogels investigated. Diffusional scaling exponents n, according to Eq. (3), for mass transfer of water into various hydrogels based on CS, M-MA and M-GU containing magnetite concentrations from 0.0 to 5.5 wt.%, ranged between 0.5430 and 0.6496. Previous studies carried out by our research group indicate that there is no variation in the water diffusion mechanism for these kinds of hydrogels, and electrostatic repulsion between ionic groups leads to expansion of the polymer network (Paulino, Belfiore, Kubota, Muniz, Almeida et al., 2011; Paulino, Belfiore, Kubota, Muniz, & Tambourgi, 2011). Boundary layer mass transfer across an expanding interface, which is consistent with isotropic swelling, provides a connection between diffusional scaling exponent n in Eq. (3), and the following scaling laws for isotropic volumetric expansion $V(t)$ of spherical hydrogels that exhibit increasing surface area $S(t)$ for interphase mass transfer of water (Belfiore, 2003);

$$\begin{aligned} V(t) &= \beta t^{\alpha} \\ S(t) &= 4\pi \left\{ \frac{3\beta}{4\pi} \right\}^{2/3} t^{2\alpha/3} \\ \frac{m(t)}{m_{\text{equilibium}}(t \Rightarrow \infty)} &= kt^n \approx D^{0.5}_{H_2O/\text{hydrogel}} t^{2\alpha/3+1/2} \\ \alpha &= \frac{3}{2}\left(n - \frac{1}{2}\right) \end{aligned} \tag{8}$$

Hence, scaling exponents $n > 0.5$ are consistent with volumetric expansion at longer time (i.e., $\alpha > 0$) as these hydrogels absorb water.

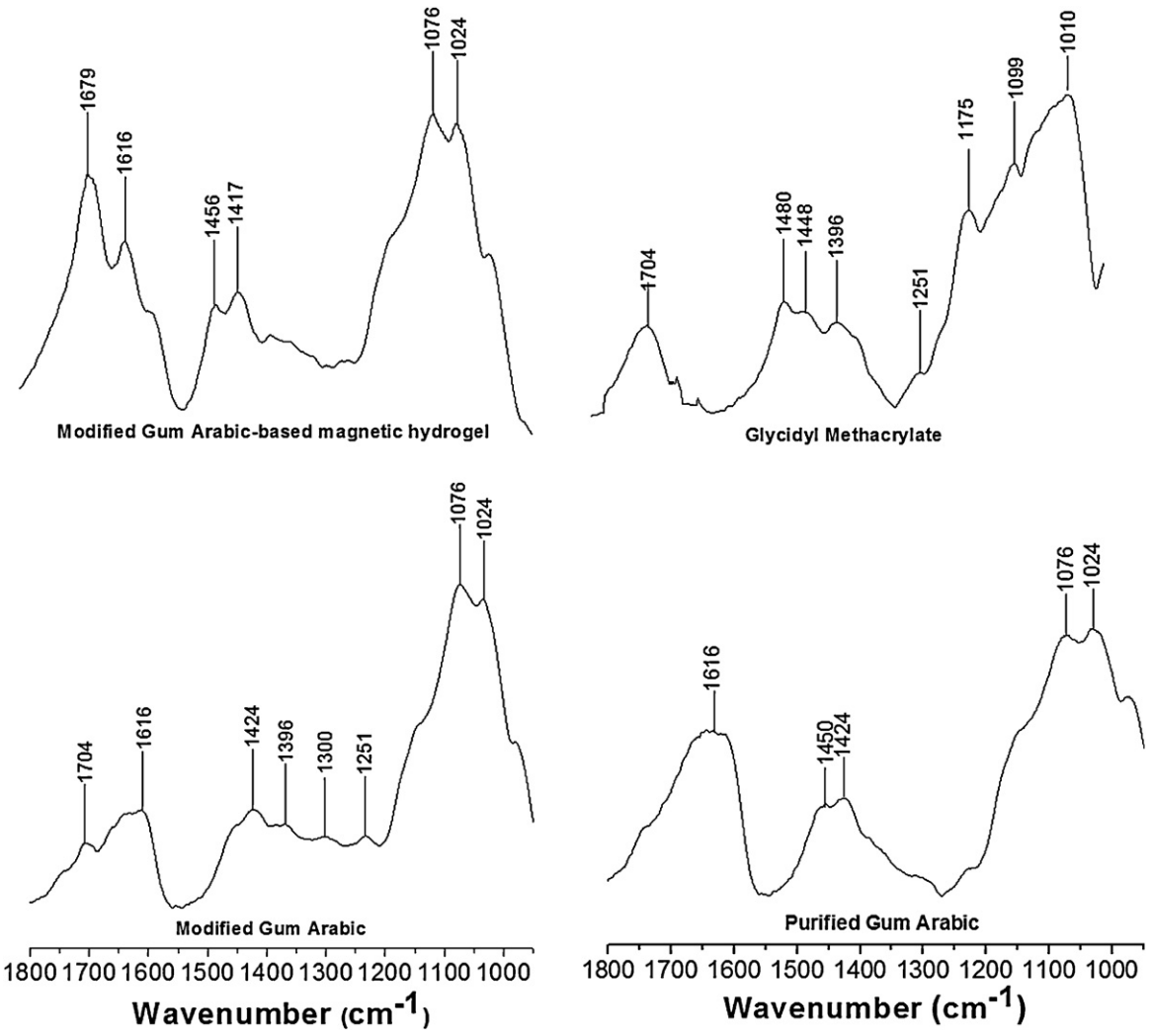

Fig. 3. Transmission FTIR spectra of GU modified with GMA, and M-GU-based hydrogels, with and without FeO:Fe_2O_3 nanoparticles.

3.2. Vibrational spectroscopy

Fig. 1 displays the FTIR spectra of CS-based hydrogels, with and without 50-nm diameter FeO:Fe_2O_3. All CS-based hydrogels exhibit carbonyl stretches (i.e., 1715–1724 cm^{-1}), characteristic of carboxylic acids, asymmetric carboxylate stretches (i.e., 1552–1574 cm^{-1}), and symmetric carboxylate stretches near 1400 cm^{-1}, due to polyacrylic acid. Chitosan-based hydrogels with FeO:Fe_2O_3 exhibit a carboxylic acid C—O stretching vibration at 1249 cm^{-1}. The amide carbonyl stretch from acetylated groups (i.e., 10%) in CS and MBA appears as a shoulder at 1650 cm^{-1} in both spectra illustrated in Fig. 1. The N—H in-plane bend of the amide group (i.e., amide II) absorbs in the region of the asymmetric carboxylate carbonyl (i.e., 1550—1600 cm^{-1}). CS-based hydrogels without FeO:Fe_2O_3 nanoparticles exhibit strong carboxylate absorptions at 1401 cm^{-1} and 1574 cm^{-1}. In comparison, CS-based magnetic hydrogels exhibit strong carboxylic acid absorptions at 1249 cm^{-1} and 1715 cm^{-1}. CS-based hydrogels with FeO:Fe_2O_3 nanoparticles reveal that the asymmetric carboxylate stretch shifts to lower wavenumbers upon chelation with iron (Kirwan, Fawell, & von Bronswijk, 2003). The absorption at 1451 cm^{-1} is, most likely, attributed to methyl groups, and NH_2 scissoring is apparent at 1322 cm^{-1}. In the presence of magnetite, the NH_2 scissoring band is dominated by the much stronger carboxylic acid C—O stretch at 1249 cm^{-1}. The absorption at 1155 cm^{-1} contains contributions from methylene scissoring and C—O—C bond vibrations in the saccharide ring. This absorption at 1155 cm^{-1} and methyl deformation at 1451 cm^{-1} are not affected by the presence of magnetite. The absorption at 1110 cm^{-1} is due to C—N stretching and vibrational modes of the saccharide rings. The absence of ammonium vibrations (e.g., asymmetric stretch at 1600 cm^{-1} and symmetric stretch at 1530 cm^{-1}) suggests that carboxylic acids might form coordination complexes with low-molecular-weight counter ions in the gel (Almodóvar, Place, Gogolski, Erickson, & Kipper, 2011; Lawrie et al., 2007). Addition of FeO:Fe_2O_3 nanoparticles might protonate some of the carboxylate groups to yield carboxylic acids, with subsequent shift to lower wavenumbers due to chelation with iron (Kirwan et al., 2003).

Fig. 2 displays the FTIR spectra of the P-MA, GMA, M-MA and M-MA-based magnetic hydrogels. The absorptions at 1371 cm^{-1} and 1649 cm^{-1} in the spectrum of P-MA correspond to COH bending vibrations, whereas the absorptions at 1452 cm^{-1} and 1420 cm^{-1} are attributed to methyl group vibrations and CH_2 scissoring, respectively. P-MA, M-MA, and M-MA-based magnetic hydrogels exhibit similar infrared absorptions between 1025 cm^{-1} and 1245 cm^{-1}. Carboxylic acid C—O stretching occurs at 1245 cm^{-1}. Absorptions between 1000 cm^{-1} and 1152 cm^{-1} are attributed to saccharide ring vibrations and ether bonds. Modification of P-MA via GMA yields a new absorption band at 1704 cm^{-1} due to carbonyl stretching of ester groups in GMA. This absorption at 1704 cm^{-1}

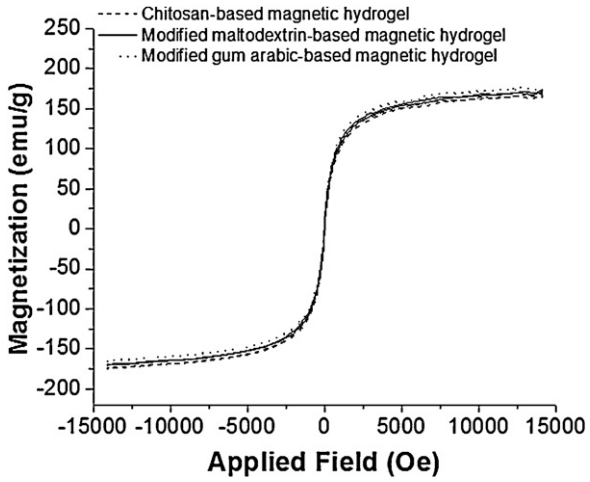

Fig. 4. Magnetization vs. applied magnetic field for magnetic hydrogels based on CS, M-MA and M-GU; magnetic hydrogels contain 1.9 wt.% $FeO:Fe_2O_3$ nanoparticles.

indicates successful modification of the polysaccharide, P-MA (Paulino, Fajardo, et al., 2011). M-MA-based magnetic hydrogels reveal carbonyl stretching vibrations at 1619 cm^{-1} and 1675 cm^{-1}. These absorptions contain contributions from amide carbonyls (i.e., 1675 cm^{-1}) and carboxylate groups (i.e., 1619 cm^{-1}), confirming the polymerization of acrylamide and acrylic acid, respectively. The peaks at 1245 cm^{-1} and 1371 cm^{-1}, due to hydroxyl groups in M-MA, shift to lower energy (i.e., 1203 cm^{-1} and 1352 cm^{-1}, respectively) as a consequence of hydrogen bonding. In contrast to the absorptions at 1249 cm^{-1} and 1552 cm^{-1} in CS-based magnetic hydrogels (see Fig. 1), the spectra of M-MA-based magnetic hydrogels do not exhibit strong contributions from the chelation of carboxylic acids by iron, suggesting that M-MA-based and CS-based hydrogels do not share the same mode of interaction with magnetite.

Fig. 3 displays the FTIR spectra of the P-GU, GMA, M-GU and M-GU-based magnetic hydrogels. The spectrum of P-GU reveals an absorption at 1616 cm^{-1} that corresponds to carbonyl stretching and COH bending in purified polysaccharides. Absorptions at 1450 cm^{-1} and 1424 cm^{-1} correspond to methyl group vibrations and CH_2 scissoring, respectively. Peaks at 1024 cm^{-1} and 1076 cm^{-1} correspond to ether bonds and saccharide ring vibrations, respectively. In the spectrum of M-GU, a new absorption at 1704 cm^{-1} is attributed to carbonyl stretching vibrations of the ester groups in GMA. The carbonyl stretching region of M-GU-based magnetic hydrogels is very similar to the analogous region in M-MA-based magnetic hydrogels (see Fig. 2). In addition to the amide carbonyl absorption at 1669 cm^{-1}, the spectra of P-GU and GU-based magnetic hydrogels are very similar, suggesting that these hydrogels do not interact strongly with magnetite.

3.3. Magnetometry

Fig. 4 displays magnetization loops [magnetization vs. applied magnetic field (B–H)] for CS-, M-MA-, and M-GU-based magnetic hydrogels containing 1.9 wt.% $FeO:Fe_2O_3$ nanoparticles. The saturation magnetization values ranged from 150 to 160 emu g^{-1}. Neither remanence nor coercivity was observed for all of these magnetic hydrogels due to the absence of hysteresis loops. This magnetic behaviour is characteristic of nanoparticulate materials embedded in hydrogels (Paulino, Fajardo, et al., 2011; Paulino et al., 2009, 2010). Therefore, it may be concluded that these natural polymer-based magnetic hydrogels exhibit nanoparticulate structures. Furthermore, $FeO:Fe_2O_3$ nanoparticles are embedded in these hydrogels via covalent bonding, exhibiting characteristics of magnetic and superparamagnetic materials (Paulino, Belfiore, Kubota, Muniz, Almeida et al., 2011; Paulino et al.,2009, 2010). Superparamagnetic properties exhibited by these hydrogels are directly related to the 50-nm size of $FeO:Fe_2O_3$ nanoparticles and their satisfactory dispersion throughout the polymeric network. If $FeO:Fe_2O_3$ nanoparticles were not sufficiently small and their

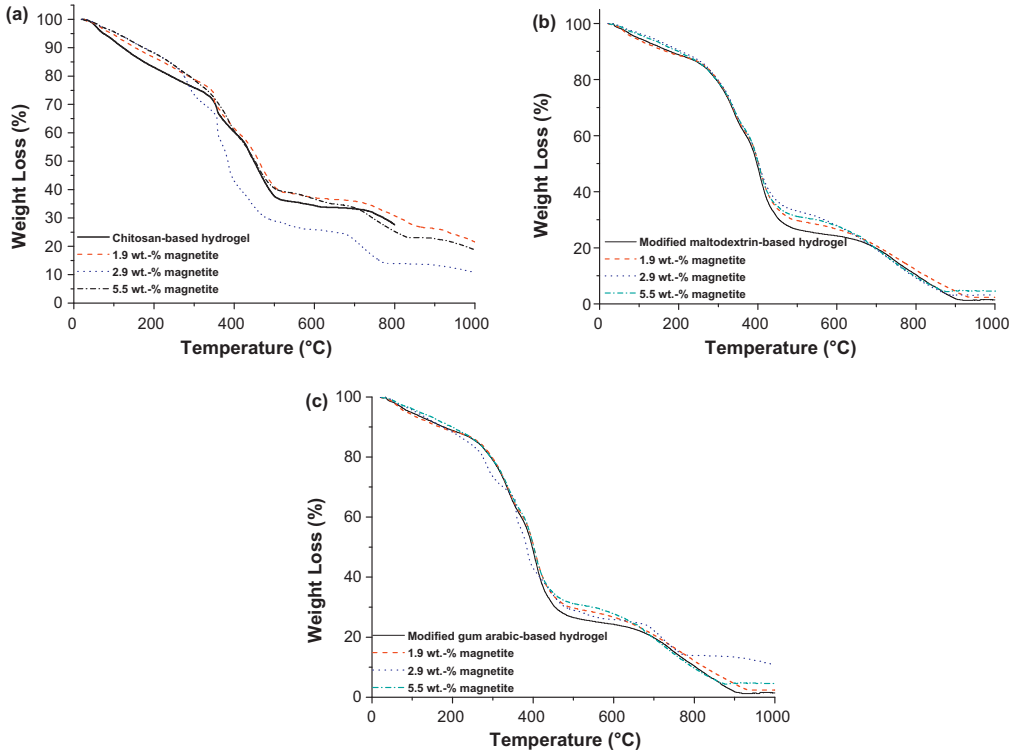

Fig. 5. Thermogravimetric analysis (TGA) of hydrogels based on CS (a), M-MA (b) and M-GU (c), with various mass fractions of $FeO:Fe_2O_3$ nanoparticles.

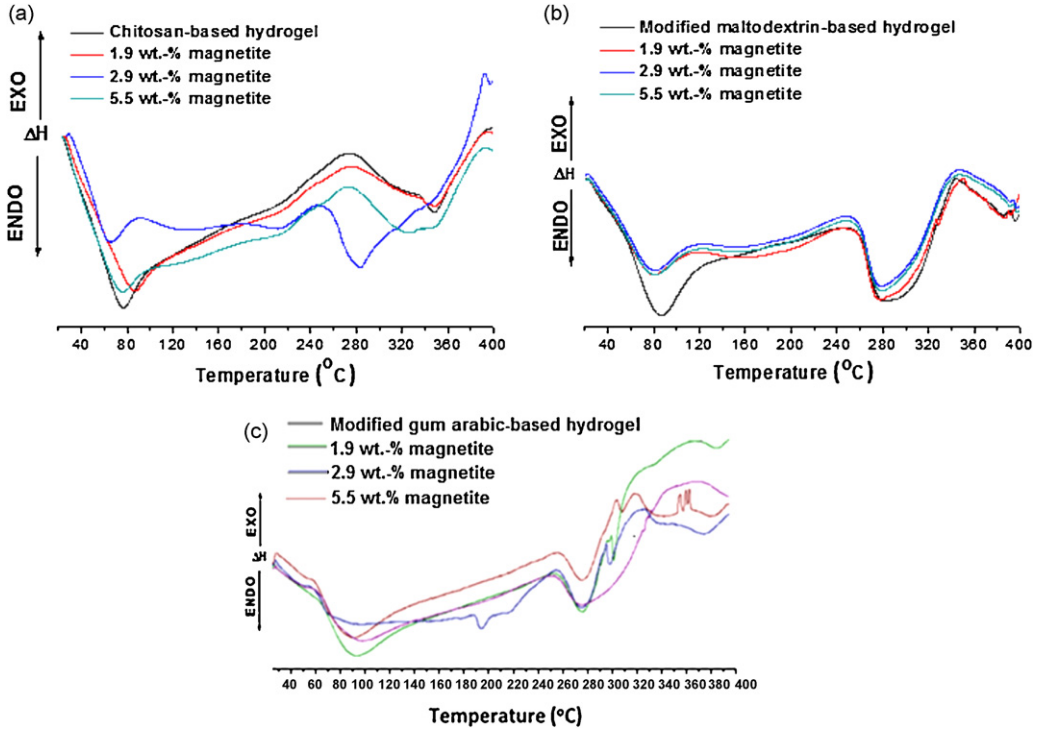

Fig. 6. DSC traces for CS-based (a), M-MA-based (b) and M-GU-based (c) hydrogels, with various mass fractions of FeO:Fe_2O_3 nanoparticles.

dispersion was poor, then a lack of either magnetization or superparamagnetic properties would be observed. Soft ferromagnetic materials with either low or no coercivity are useful for electronic devices. In many applications, small hysteresis loops are driven around points in the *B–H* plane. Loops near the origin have greater magnetic permeability (Paulino, Belfiore, Kubota, Muniz, & Tambourgi, 2011; Paulino et al., 2009, 2010).

3.4. Thermal analysis (TGA and DSC)

Fig. 5 shows TGA curves for magnetic hydrogels based on CS (a), M-MA (b) and M-GU (c). All hydrogels exhibit mass loss in two different temperature ranges. The initial loss of mass in the vicinity of 90 °C is attributed to water. Even after drying, water molecules might be bound to natural polymer-based hydrogels due to their hydration features, such as hydrophilicity and supramolecular structures that encapsulate water (Kittur, Harish, Udaya, & Tharanathan, 2002; Ostrowska-Czubenko & Gierszewska-Drużyńska, 2009). Thermal degradation of natural polymer-based hydrogels in the second stage involves a two-step mechanism over the following range of temperatures: 250–500 °C. Similar results have been reported previously (Kittur et al., 2002; Ostrowska-Czubenko & Gierszewska-Drużyńska, 2009). Natural polymer degradation begins with random cleavage of glycoside bonds, followed by decomposition, which generates low-molecular-weight acetic, butyric, and fatty acids (Lewandowska, 2009; Neto et al., 2005; Ostrowska-Czubenko & Gierszewska-Drużyńska, 2009; Rueda, Secall, & Bayer, 1999). Thermal degradation of magnetic hydrogels based on M-MA and M-GU occurs over similar temperature ranges. In general, water loss is less abundant in hydrogels that contain higher magnetite concentrations, due to attractive interactions between CS polar functional groups and water in denser networks where void volume is occupied by well-dispersed FeO:Fe_2O_3 nanoparticles. Previous FTIR studies have reported that

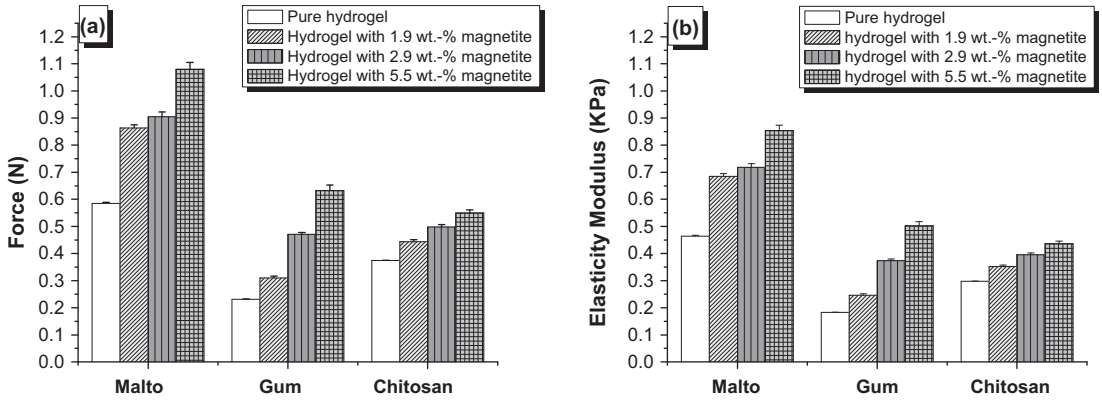

Fig. 7. Compressive forces required to achieve 10% compressive strain in polysaccharide hydrogels with various mass fractions of FeO:Fe_2O_3 nanoparticles (a), and the corresponding compressive modulus of elasticity according to Eq. (4) (b).

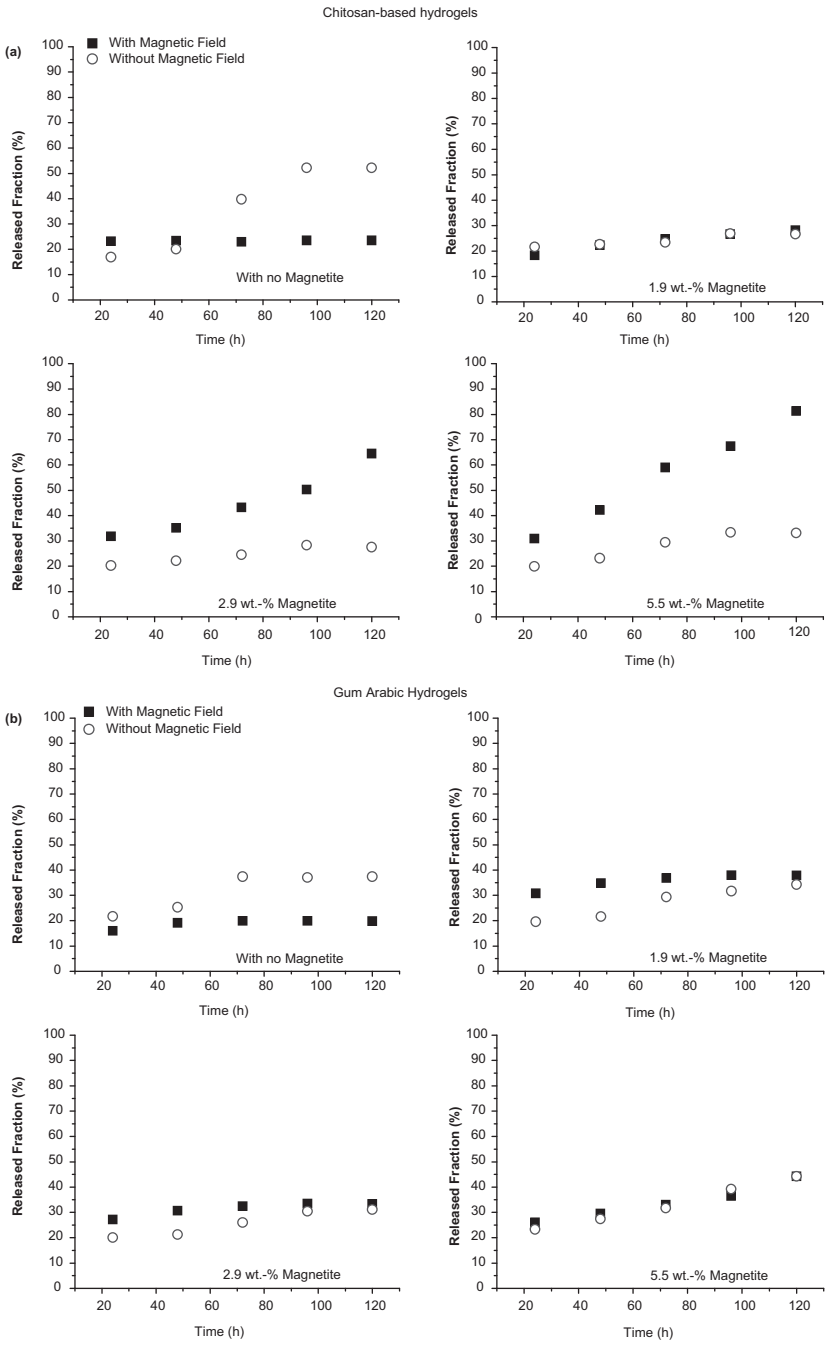

Fig. 8. Remote-controlled release of CUR from polysaccharide hydrogels that contain various mass fractions of FeO:Fe_2O_3 nanoparticles, with and without an external magnetic field (350 T).

interactions between water molecules and hydroxyl groups are stronger than water-amine interactions (Neto et al., 2005). Thermal stability increases when these hydrogels contain higher concentrations of magnetite.

Fig. 6 displays the DSC curves for magnetic hydrogels based on CS (a), M-MA (b) and M-GU (c). Chitosan hydrogels with and without magnetite exhibit broad endothermic transitions between 40 °C and 120 °C in Fig. 6a due to loss of volatile compounds (such as free water), probably occurring in harmony with network relaxation. Exothermic transitions between 200 °C and 300 °C are attributed to thermal degradation of the natural polymer, which exhibits a complex dehydration process of the saccharide rings, followed by decomposition of the CS backbone (Lewandowska, 2009; Neto et al., 2005; Rueda et al., 1999). Fig. 6b displays DSC curves for M-MA-based hydrogels, revealing two endothermic transitions in all cases. The lower-temperature endotherm between 40 °C and 120 °C is attributed to the evolution of unbound water from the hydrogel matrix. The higher-temperature endotherm between 220 °C and 320 °C is attributed to thermal decomposition of the natural polymer. Fig. 6c displays DSC curves for M-GU-based hydrogels, exhibiting one endothermic and one exothermic transition. The endothermic peak is due to water evaporation, while the exothermic peak corresponds to M-GU degradation.

3.5. Stress vs. strain under compressive loading

Fig. 7 summarizes the (a) compressive forces required to deform swollen hydrogels by 10% (i.e., compression ratio of 0.9 via Eq. (5)),

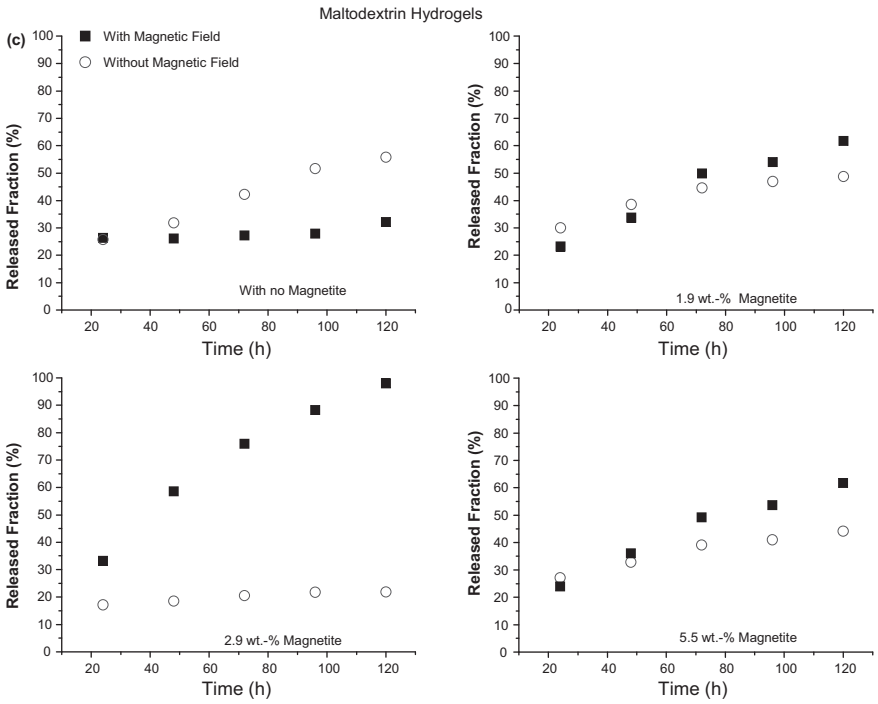

Fig. 8. (*Continued*).

and (b) compressive elastic moduli via stress–strain data according to Eq. (4). As observed in Fig. 7a, the compressive forces required to achieve 10% compressive strain are proportional to the FeO:Fe_2O_3 mass fraction in these magnetic hydrogels. Similar behaviour was observed for all three types of hydrogels. Higher FeO:Fe_2O_3 mass fractions increase the compressive moduli. Compressive stress applied to swollen magnetic hydrogels to achieve 10% compressive strain was between 1.5-fold and 3-fold greater than those stresses applied to hydrogels without magnetite. Hence, these hydrogels that contain well-dispersed FeO:Fe_2O_3 nanoparticles are magnetically responsive and exhibit superior resistance to deformation under compression. Data in Fig. 7b reveal that M-MA-based hydrogels exhibit larger compressive moduli than those for the other two types of hydrogels.

3.6. *In vitro controlled release of curcumin*

Fig. 8 displays CUR controlled release profiles from FeO:Fe_2O_3-loaded hydrogels based on CS (a), M-MA (b) and M-GU (c), with and without the application of a 350-T magnetic field. The release of CUR was monitored for approximately 120 min, revealing effects from (a) the presence of magnetite in these hydrogels, and (b) the application of an external field. For hydrogels without magnetite, the fraction of CUR released was greater under zero-field conditions. However, an increase in the fraction of CUR released from magnetic hydrogels occurred in the presence of the field. This latter result is attributed to electrostatic repulsions between ionic groups in these modified natural polymers and AAc or AAm groups that (a) destabilize hydrogel structure, and (b) allow solute diffusion out-of the polymer matrix. For hydrogels containing 1.9, 2.9 and 5.5 wt.% magnetite, the release of CUR is larger in the presence of the field as a consequence of magnetic interactions and hydrogel deswelling (Paulino, Fajardo, et al., 2011; Paulino et al., 2009, 2010). Fig. 8a reveals significant field-induced increases in the fraction of CUR released from CS-based hydrogels that contain larger mass fractions of well-dispersed FeO:Fe_2O_3 nanoparticles. Magnetic hydrogels based on M-GU M-MA (Fig. 8b) and M-MA (Fig. 8c) exhibit smaller field-induced CUR release, relative to CS-based hydrogels. This is consistent with results from FTIR spectroscopy, suggesting that FeO:Fe_2O_3 interacts more strongly with amine groups in CS relative to nanoparticle interactions with functional groups in M-MA and M-GU. All hydrogels investigated herein are attractive for remote-controlled release of CUR, via consideration of FeO:Fe_2O_3 nanoparticle mass fraction, magnetic field strength, and the hydrogel functional groups that interact with magnetite.

4. Conclusions

Polysaccharide hydrogels, with and without magnetic properties, have been prepared by conventional methods and characterized by infrared spectroscopy, magnetometry, thermogravimetry, compressive stress–strain testing, and swelling kinetics. FTIR analysis confirmed the efficiency of the polysaccharide-modifying process and cross-linking reactions in the presence of magnetite. Superparamagnetic properties of these hydrogels are a direct consequence of the 50-nm size of FeO:Fe_2O_3 nanoparticles and their satisfactory dispersion throughout the polymeric network. Thermal stability and mechanical resistance increase when these hydrogels contain larger mass fractions of magnetite. Transient diffusion of water was analyzed via boundary layer mass transfer across an expaning hydrogel interface, in support of swelling kinetic studies. The degree of swelling in these polysaccharide hydrogels is reduced in the presence of FeO:Fe_2O_3 nanoparticles, but larger mass fractions of magnetite yield hydrogels that exhibit magnetic sensitivity for remote-controlled release of curcumin in the presence of an external magnetic field. Field-induced release of curcumin, which is an anti-cancer drug, demonstrates that polysaccharide hydrogels with finely dispersed FeO:Fe_2O_3 nanoparticles are useful for cancer treatment.

Acknowledgments

AT Paulino and EB Tambourgi thank the State of São Paulo Research Foundation (FAPESP, Brazil) for the post-doctorate

fellowship (Process No. 2008/00285-7). AT Paulino is grateful to the Coordination of Improvement of Higher Education Personnel (CAPES, Brazil) for the fellowship (Process No. 5267/09-9) to support his post-doctoral research experience with LA Belfiore and MJ Kipper at Colorado State University in Fort Collins, CO, USA.

References

Almodóvar, J., Place, L. W., Gogolski, J., Erickson, K., & Kipper, M. J. (2011). Layer-by-layer assembly of polysaccharide-based polyelectrolyte multilayers: A spectroscopic study of hydrophilicity, composition, and ion pairing. *Biomacromolecules*, *12*, 2755–2765.

Arizaga, A., Ibarz, G., & Piñol, R. (2010). Stimuli-responsive poly(4-vinyl pyridine) hydrogel nanoparticles: Synthesis by nanoprecipitation and swelling behavior. *Journal of Colloid Interface Science*, *348*, 668–672.

Bajpai, A. K., Shukla, S. K., Bhanu, S., & Kankane, S. (2008). Responsive polymers in controlled drug delivery. *Progress in Polymer Science*, *33*, 1088–1118.

Baolin, G., Anna, F-W., & Ann-Christine, A. (2011). Versatile functionalization of polyester hydrogels with electroactive aniline oligomers. *Journal of Polymer Science: Polymer Chemistry*, *49*, 2097–2105.

Belfiore, L. A. (2003). *Transport phenomena for chemical reactor design*. Wiley., p. 327.

Brazel, C. S., & Peppas, N. A. (1999). Mechanisms of solute and drug transport in relaxing, swellable, hydrophilic glassy polymers. *Polymer*, *40*, 3383–3398.

Chaterji, S., Kwon, I. K., & Park, K. (2007). Smart polymeric gels: Redefining the limits of biomedical devices. *Progress in Polymer Science*, *32*, 1083–1122.

Chatterjee, J., Haik, Y., & Jen, C. (2003). Biodegradable magnetic gel: Synthesis and characterization. *Colloid Polymer Science*, *281*, 892–896.

Deligkaris, K., Tadele, T. S., Olthuis, W., & van den Berg, A. (2010). Hydrogel-based devices for biomedical applications. *Sensor Actuator B*, *147*, 765–774.

Deng, Y., Yang, W., Wang, C., & Fu, S. (2003). A novel approach for preparation of thermoresponsive polymer magnetic microspheres with core–shell structure. *Advanced Materials*, *15*, 1729–1732.

Friedrich, T., Trinker, A., & Tieke, B. (2010). Functionalization of hydrogels based on N-isopropyl-acrylamide and cationic surfactant monomers upon electrostatic self-assembly. *Macromolecular Symposia*, *298*, 57–63.

Gutowska, A., Bae, Y. H., Jacobs, H., Feijen, J., & Kim, S. W. (1994). Thermosensitive interpenetrating polymer networks: Synthesis, characterization, and macromolecular release. *Macromolecules*, *27*, 4167–4175.

Kirwan, L. J., Fawell, P. D., & von Bronswijk, W. (2003). In situ FTIR-ATR examination of poly(acrylic acid) adsorbed onto hematite at low pH. *Langmuir*, *19*, 5802–5807.

Kittur, F. S., Harish, P. K. V., Udaya, S. K., & Tharanathan, R. N. (2002). Characterization of chitin chitosan and their carboxymethyl derivatives by differential scanning calorimetry. *Carbohydrate Polymers*, *49*, 185–193.

Lau, K. Y., Cheng, L., Su, Z. Q., & Varadan, V. K. (2009). Smart composite materials: Selected papers from the international conference on multifunctional materials and structures (MFMS 08) (Hong Kong, 28–31 July 2008). *Smart Materials and Structures*, *18*, art. no. 070201.

Lawrie, G., Keen, I., Drew, B., Chandler-Temple, A., Rintoul, L., Fredericks, P., et al. (2007). Interactions between alginate and chitosan biopolymers characterized using FTIR and XPS. *Biomacromolecules*, *8*, 2533–2541.

Lewandowska, K. (2009). Miscibility and thermal stability of poly(vinyl alcohol)/chitosan mixtures. *Thermochimica Acta*, *493*, 42–48.

Liu, Y., Ibricevic, A., Cohen, J. A., Cohen, J. L., Gunsten, S. P., Fréchet, J. M. J., et al. (2009). Impact of hydrogel nanoparticle size and functionalization on in vivo behavior for lung imaging and therapeutics. *Molecular Pharmaceutics*, *6*, 1891–1902.

Mahkam, M. (2010). Modified chitosan cross-linked starch polymers for oral insulin delivery. *Journal of Bioactive and Compatible Polymers*, *25*, 406–418.

Neto, C. G. T., Giacometti, J. A., Job, A. E., Ferreira, F. C., Fonseca, J. L. C., & Pereira, M. R. (2005). Thermal analysis of chitosan based networks. *Carbohydrate Polymers*, *62*, 97–103.

Oh, J. K., Drumright, R., Siegwart, D. J., & Matyjaszewski, K. (2008). The development of microgels/nanogels for drug delivery applications. *Progress in Polymer Science*, *33*, 448–477.

Ostrowska-Czubenko, J., & Gierszewska-Drużyńska, M. (2009). Effect of ionic crosslinking on the water state in hydrogel chitosan membranes. *Carbohydrate Polymers*, *77*, 590–598.

Paulino, A. T., Belfiore, L. A., Kubota, L. T., Muniz, E. C., Almeida, V. C., & Tambourgi, E. B. (2011). Effect of magnetite on the adsorption behavior of Pb(II), Cd(II), and Cu(II) in chitosan-based hydrogels. *Desalination*, *275*, 187–196.

Paulino, A. T., Belfiore, L. A., Kubota, L. T., Muniz, E. C., & Tambourgi, E. B. (2011). Efficiency of hydrogels based on natural polysaccharides in the removal of Cd^{2+} ions from aqueous solutions. *Chemical Engineering Journal*, *168*, 68–76.

Paulino, A. T., Fajardo, A. R., Junior, A. P., Muniz, E. C., & Tambourgi, E. B. (2011). Two-step synthesis and properties of a magnetic-field-sensitive modified maltodextrin-based hydrogel. *Polymer International*, *60*, 1324–1333.

Paulino, A. T., Guilherme, M. R., Almeida, E. A. M. S., Pereira, A. G. B., Muniz, E. C., & Tambourgi, E. B. (2009). One-pot synthesis of a chitosan-based hydrogel as a potential device for magnetic biomaterial. *Journal of Magnetism and Magnetic Materials*, *321*, 2636–2642.

Paulino, A. T., Guilherme, M. R., Mattoso, L. H. C., & Tambourgi, E. B. (2010). Smart hydrogels based on modified gum arabic as a potential device for magnetic biomaterial. *Macromolecular Chemistry and Physics*, *211*, 1196–1205.

Rueda, D. R., Secall, T., & Bayer, R. K. (1999). Differences in the interaction of water with starch and chitosan films as revealed by infrared spectroscopy and differential scanning calorimetry. *Carbohydrate Polymers*, *40*, 49–56.

Shalviri, A., Liu, Q., Abdekhodaie, M. J., & Wu, X. Y. (2010). Novel modified starch–xanthan gum hydrogels for controlled drug delivery: Synthesis and characterization. *Carbohydrate Polymers*, *79*, 898–907.

Simionato, J. I., Paulino, A. T., Garcia, J. C., & Nozaki, J. (2006). Adsorption of aluminium from wastewater by chitin and chitosan produced from silkworm chrysalides. *Polymer International*, *55*, 1243–1248.

Snyder, R. L., Nguyen, V. Q., & Ramanujan, R. V. (2010a). Design parameters for magneto-elastic soft actuators. *Smart Materials and Structures*, *19*, art. no. 055017.

Snyder, R. L., Nguyen, V. Q., & Ramanujan, R. V. (2010b). The energetics of magnetoelastic actuators is analogous to phase transformations in materials. *Acta Materialia*, *58*, 5620–5630.

Song, F., Zhang, L. M., Shi, J. F., & Li, N. N. (2010). Novel casein hydrogels: Formation structure and controlled drug release. *Colloids and Surfaces B: Biointerfaces*, *79*, 142–148.

van Dijk-Wolthuis, W. N. E., Franssen, O., Talsma, H., van Steenbergen, M. J., Kettenes-van den Bosch, J. J., & Hennink, W. E. (1995). Synthesis, characterization and polymerization of glycidyl methacrylate derivatized dextran. *Macromolecules*, *28*, 6317–6322.

van Dijk-Wolthuis, W. N. E., Kettenes-van den Bosch, J. J., van der Kerk-van Hoof, A., & Hennink, W. E. (1997). Reaction of dextran with glycidyl methacrylate: An unexpected transesterification. *Macromolecules*, *30*, 3411–3413.

Wang, W., Kang, Y., & Wang, A. (2010). Synthesis, characterization and swelling properties of guar gum-g-poly(sodium acrylate-co-styrene)/muscovite superabsorbent composites. *Science and Technology of Advanced Materials*, *11*, art. no. 025006.

Zhang, Y. X., Wu, F. P., Li, M. Z., & Wang, E. J. (2005). pH switching on-off semi-IPN hydrogel based on cross-linked poly(acrylamide-*co*-acrylic acid) and linear polyallyamine. *Polymer*, *46*, 7695–7700.